Materials Today Bio 22 (2023) 100752

Contents lists available at ScienceDirect

Materials Today Bio

journal homepage: www.journals.elsevier.com/materials-today-bio

Rapidly *in situ* forming an injectable Chitosan/PEG hydrogel for intervertebral disc repair

Lin Huang [a], Wantao Wang [a,b], Yiwen Xian [a], Lei Liu [a], Jinghao Fan [a], Hongmei Liu [a,**], Zhaomin Zheng [b,***], Decheng Wu [a,*]

[a] *Guangdong Provincial Key Laboratory of Advanced Biomaterials, Department of Biomedical Engineering, Southern University of Science and Technology, Shenzhen, 518055, China*

[b] *Department of Spine Surgery, The First Affiliated Hospital, Sun Yat-Sen University, Guangzhou, 510275, China*

ARTICLE INFO

Keywords:
Chitosan
PEG
Injectable hydrogel
Tissue engineering
Intervertebral disc repair

ABSTRACT

Intervertebral disc (IVD) degeneration occurred with the increasing age or accidents has puzzled peoples in daily life. To seal IVD defect by injectable hydrogels is a promising method for slowing down IVD degeneration. Herein, we reported a rapidly *in situ* forming injectable chitosan/PEG hydrogel (CSMA-PEGDA-L) through integrating photo-crosslink of methacrylate chitosan (CSMA) with Schiff base reaction between CSMA and aldehyde polyethylene glycol (PEGDA). The CSMA-PEGDA-L possessed a stronger compressive strength than the photo-crosslinked CSMA-L hydrogel and Schiff-base-crosslinked CSMA-PEGDA hydrogel. This chitosan/PEG hydrogel showed low cytotoxicity from incubation experiments of nucleus pulpous cells. When implanted on the punctured IVD of rat's tail, the CSMA-PEGDA-L hydrogel could well retard the progression of IVD degeneration through physical plugging, powerfully proven by radiological and histological evaluations. This work demonstrated the strategy of *in situ* injectable glue may be a potential solution for prevention of IVD degeneration.

1. Introduction

Intervertebral disc (IVD) degeneration caused by aging or accidents has disturbed peoples of all ages especially for elders around the world. IVD degeneration always leads to some prevalent symptoms such as low back pain (LBP), dysfunction on movement even disability, which greatly increased the socioeconomic burden [1,2]. Clinical treatment for IVD degeneration always involves administrating the anti-inflammatory or analgesia drugs in an early stage, while surgical operation has to be carried out when patients are suffered from severe IVD degeneration. Conventional surgical interventions aim to remove the pathological nucleus pulposus (NP) or annulus fibrosus (AF) to prevent the nerve root from being compressed by the deteriorated NP as well as AF [3,4]. Immediately as the painfulness can be relieved in some extent, however, due to the intricate structure and unique biologic milieu *in vivo* of IVD, NP or AF is hard to replenish, resulting in the recurrence of herniation after surgery therapy [5,6]. Specially, the unique lamellar structure of collagen fibers in AF makes it very difficult to be well reorganized for reconstructing the biomechanical function of IVD [7]. Rigid artificial IVD prosthesis is a current popular solution for replacing IVD, but it is lack of regenerative capability [8]. To overcome these challenges, many efforts have been proposed to mimic or reconstruct IVD function, and similar mechanical performances to native IVD are realized [9–11]. Wherein, the injectable hydrogels are promising biomaterials for treating the degenerated IVD after discectomy because of their flexible adaptability to irregular wounds, and high loaded capacity for therapeutic drugs [12–14]. However, low gelation speed, sophisticated manufactures, or poor biocompatibility of the existed injectable hydrogels are still critical issues for hindering clinical use in IVD treatment.

Chitosan, a natural linear polysaccharide with β-1, 4-glucosamine structure similar to hyaluronic acid which is an essential component in extracellular matrix (ECM) and articular cartilage fluid, has been widely used as biomaterial scaffolds in tissue engineering due to its high biocompatibility, degradability as well as low immunogenicity [15,16]. Nevertheless, the inherent strong hydrogen bonds make chitosan

* Corresponding author.
** Corresponding author.
*** Corresponding author.
E-mail addresses: liuhm@sustech.edu.cn (H. Liu), zhengzm1@163.com (Z. Zheng), wudc@sustech.edu.cn (D. Wu).

https://doi.org/10.1016/j.mtbio.2023.100752
Received 1 June 2023; Received in revised form 19 July 2023; Accepted 27 July 2023
Available online 28 July 2023

difficult to be directly used as regenerative biomaterials in form of *in situ* gelling unless modify chitosan into water soluble state. Fortunately, the amino groups on chitosan can provide reactive positions to fabricate dynamic hydrogels [17–19], or serve as an adhesive bridge between hydrogel and tissue [20,21]. Conventionally, the pure injectable chitosan hydrogel is always in low mechanical strength thus presents to limited applications such as wound dressings [22,23], or drug releasing [24]. Chemical modifications or crosslinking additives are potential strategies to improve the mechanical strength of injectable chitosan hydrogels [25–28]. Polyethylene glycol (PEG) has been clinically used as a traditional biomedical hydrogel matrix in early 1960s because of its high biocompatibility to mammalian cells and tissues [29]. Functional groups such as diacrylate, aldehyde, thiol, or *N*-hydroxy succinimide are always tailored on the end of PEG chain to form a crosslinking point for designing injectable hydrogels [30,31]. Although many reported injectable chitosan/PEG hybrid hydrogels exhibit good therapeutic efficiency as tissue engineering scaffolds [32–36], to combine fast gelation and improved mechanical strength together still remains a challenge for injectable chitosan hydrogels. The inherently abundant amino groups and introduced functional binding groups on chitosan chain can synergistically strengthen the hydrogel network and rapidly *in situ* form the hydrogel, which may be applicable in high stress dependent tissue engineering scaffold [37].

Herein, we reported a rapidly *in situ* forming injectable chitosan/PEG hydrogel through two-syringes mixing of methacrylate chitosan (CSMA) and PEGDA for retarding the degeneration of IVD (Scheme 1). The chitosan hydrogel (CSMA-L) showed fast gelation under 405 nm light irradiation, and the dynamic imine bond of Schiff base reaction could further improve the mechanical strength of chitosan/PEG hydrogel (CSMA-PEGDA-L). The hydrogel was effective in promoting the proliferation of nucleus pulpous cells. *In vivo* experiment on rat's tail claimed the hydrogel could well seal the punctured IVD, protecting it from further deterioration. Radiology and histology evaluations on the IVD of rat's tail distinctly showed the importance of chitosan/PEG hydrogel in retarding the IVD degeneration.

2. Results and discussion

The inherent undissolved property of chitosan in aqueous or most organic solvents impeded its wide applications, and modifications on chitosan chains based on amine group at C2 position or hydroxyl group at C3 and C6 position are always used to fabricate the water-soluble chitosan-based materials for further use especially in biomedical applications [38]. As illustrated in Fig. 1a, chitosan could be directly dissolved in water or PBS at neutral pH for biological applications after grafted with methacrylic group. The chemical shifts at 5.6 ppm, 5.3 ppm or 1.9 ppm presented the ethylene (=CH_2) or methyl (-CH_3) of methacrylic group (Fig. 1b), suggesting the successful synthesis of methacrylate chitosan (CSMA) [39]. With the methacrylic anhydride amount increased, the degree of methacrylic group on chitosan were also enhanced from 18% (CSMA1), 21% (CSMA2), to 27% (CSMA3) according to the portion of chemical shifts between 4.5 and 2.5 ppm. FT-IR spectra also showed the successful synthesis of CSMA (Fig. 1c). The stretching vibration at 1730 cm^{-1} (C═O) had no obvious change but the amide group (-CO-NH-) at 1560 cm^{-1} significantly increased especially in CSMA3, which indicated the graft of methacrylic group on chitosan. The Zeta potentials of chitosan and different CSMA samples were 13.1, 31.0, 40.2, and 47.2 mV respectively (Fig. 1d), also indicating an increase in the substitute content of methacrylic group on chitosan chain from CSMA1 to CSMA3. Because the inherent hydrogen bonds in chitosan were destroyed through introducing methacrylate group, the dissolution ability of CSMA in water was obviously improved [39]. The CSMA can be quickly *in situ* gelled under blue light irradiation and is beneficial to cell adhesion, but the mechanical strength of injectable hydrogel is always lower than that of the preformed gel [40]. The amino group on chitosan and aldehyde group on PEG can quickly form an imine group (-N═CH-) through Schiff base reaction under mild environment, which may synergistically enhance the strength of CSMA hydrogel. The hydroxyl group on PEG chain could be easily substituted by 4-formylbenzoic acid to form the terminal dialdehyde group modified PEG, coded as PEGDA (Fig. 1e). Both the chemical shifts at 10.1 ppm (-CHO), 8.2 ppm and 7.9 ppm (aromatic hydrogen atom) in Fig. 1f, and stretching vibration at 1706 cm^{-1} (C═O) in Fig. 1g well showed the successful synthesis of PEGDA. The typical absorption at 256 nm of aromatic group in ultra violet spectra were obvious in PEGDA while not in PEG (Fig. 1h). PEGDA can act as a crosslinker for CSMA to construct a dual network hydrogel with existence of 405 nm light and initiator. The light initiator in this work preferred to LAP (Fig. S1), because it has already been proved to be much safer than Irgacure2959 when applied in cell incubation by Fairbanks et al. [41].

The conceptional rapidly *in situ* forming injectable hydrogel constructed by CSMA and PEGDA was illustrated in Fig. 2a. Firstly, both

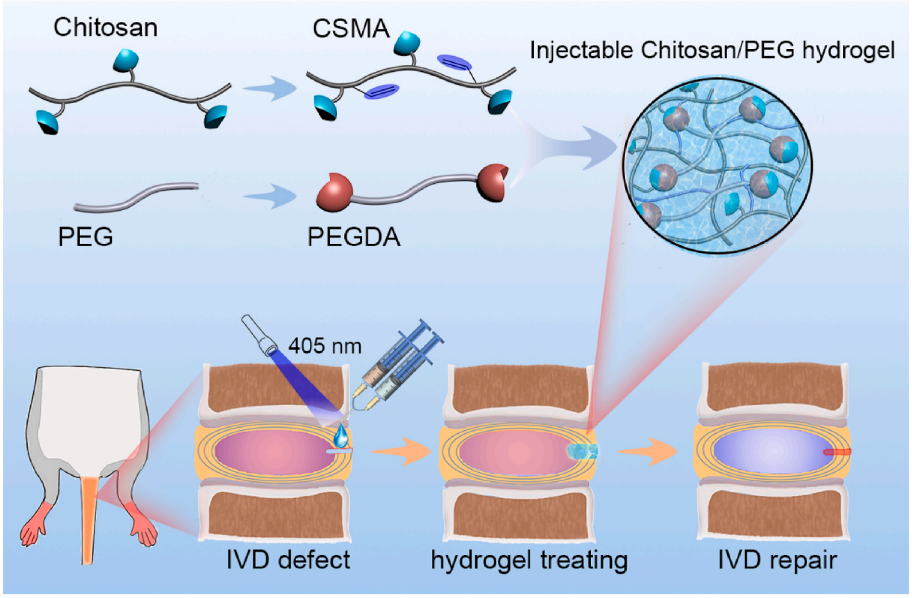

Scheme 1. Illustration of the rapidly *in situ* forming injectable chitosan/PEG hydrogel for intervertebral disc degeneration repair.

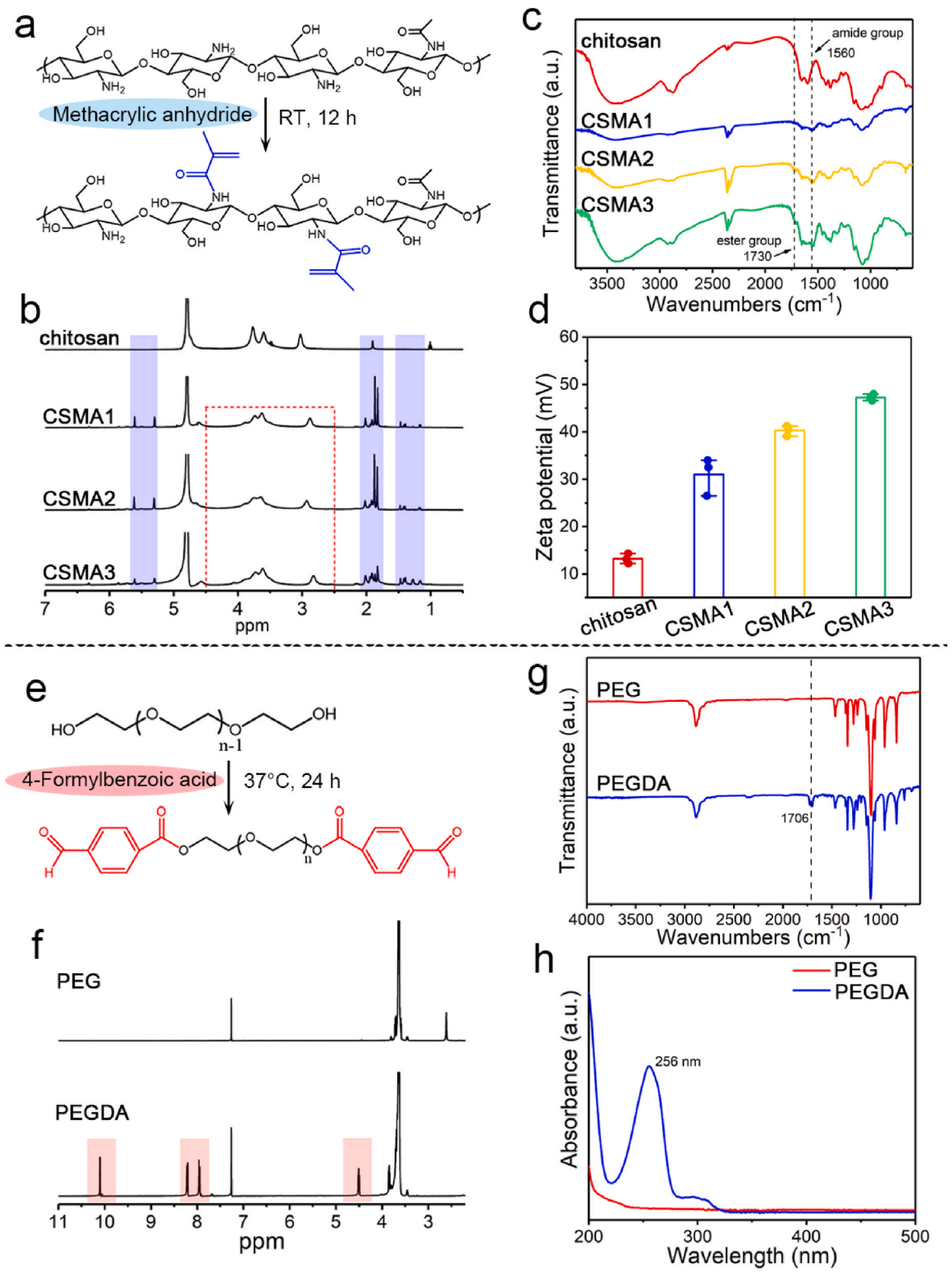

Fig. 1. Synthesis and characterization of methacrylate chitosan (CSMA) and dialdehyde group modified polyethylene glycol (PEGDA). Synthetic route (a), ^{1}H NMR spectra (b), FT-IR spectra (c) and Zeta potentials (d) of chitosan with different substitution degree of methacrylic groups (n = 3). Synthetic route (e), and ^{1}H NMR (f), FT-IR (g) and UV–vis spectra (h) of PEG and PEGDA.

water-soluble CSMA and PEGDA were dissolved in water in a certain weight percent, and then homogeneously mixed through two-channel syringes for producing a dynamic covalently crosslinked hydrogel (Gel1, CSMA-PEGDA). After irradiation by 405 nm blue light in seconds, the CSMA could further quickly polymerize, and ultimately form a dual network hydrogel (Gel2, CSMA-PEGDA-L). The hydrogel consisted of CSMA and PEGDA through dynamic Schiff base reaction almost needed 60 s, while the gelation process was greatly accelerated with light

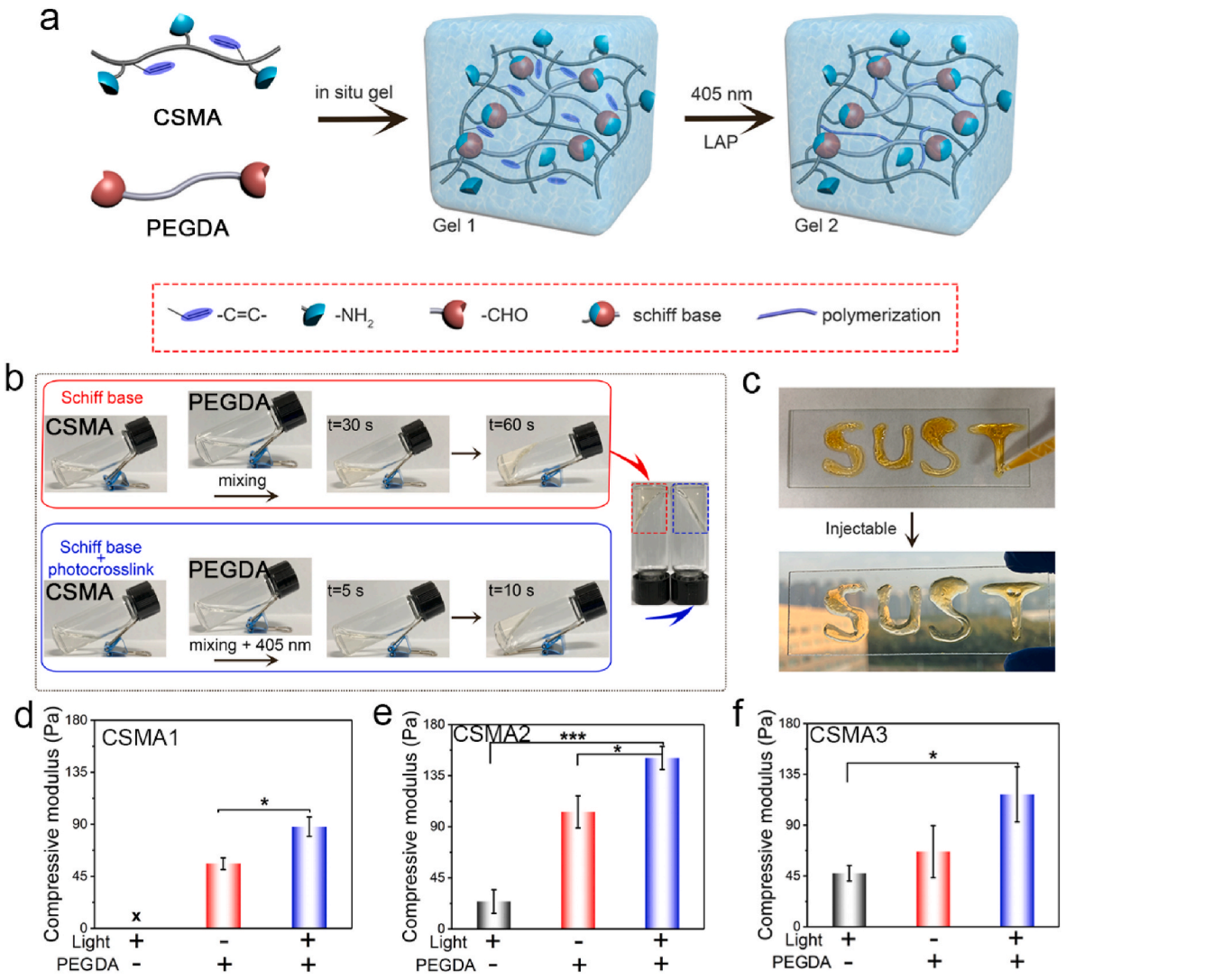

Fig. 2. Preparation and presentation of chitosan/PEG hydrogels. Schematic illustration of CSMA-PEGDA (Gel 1) and CSMA-PEGDA-L (Gel 2) (a). Digital photos for showing the comparison between Schiff base reaction hydrogel and dual crosslink hydrogel through simple vial inversion method (b). Photos for proving the injectability of CSMA-PEGDA hydrogel stained by orange dye (c). Statistics of compressive modulus on different CSMA hydrogels in the absence or presence of light or PEGDA (d)–(f) ($n = 3$, ***$p < 0.001$, *$p < 0.05$). (For interpretation of the references to colour in this figure legend, the reader is referred to the Web version of this article.)

irradiation which merely about 10 s according to the vial inversion experiment (Fig. 2b). The hydrogel was also proved to be smoothly injectable as "SUST" characters (Fig. 2c), which can further be strengthened through light-mediated crosslinking. To be noted, the mechanical property of the dual crosslink hydrogel was mainly influenced by both the content of polymer matrix and substituted degree of methacrylate group on chitosan. As for the single CSMA-L hydrogel, the mechanical strength was proportional to the substituted degree of methacrylic group (MA), as visually shown in Fig. S2. Compared to CSMA3-L, the hydrogel with low substitution degree of MA on chitosan (CSMA1-L) even cannot be well-shaped under a concentration of 1 wt % because the low crosslink density cannot maintain the network. However, higher crosslink density in CSMA3-L may not present lower swelling ratio as the solubility of chitosan was also increased when the substitution of MA on chitosan was enhanced (Fig. S3). This meant two factors, crosslink density and solubility of CSMA, were responsible for the swelling property of CSMA-L single network hydrogel. Meanwhile, the dynamic covalent crosslink hydrogel of CSMA-PEGDA also presented high hydrophilic performance, which can be fully hydrated in minutes, and these results were even obvious in CSMA3-PEGDA group (Fig. S3). When these two crosslink manners were combined together, the dual network hydrogel exhibited a lower swelling ratio compared to single network. Although the compressive stress in different CSMA groups with light or Schiff base crosslink did not show significant difference, ranging from 20 to 50 kPa (Fig. S4), the compressive modulus was actually enhanced in dual network hydrogel group. The introduction of PEGDA improved the hydrogel modulus, calculated at 56 Pa, 103 Pa and 67 Pa for CSMA1-3/PEGDA, and further increased to 88 Pa, 151 Pa and 117 Pa after 405 nm light irradiation (Fig. 2d–f). The compressive stress and modulus of CSMA and PEGDA hybrid gels were determined by the degree of MA and the content of PEGDA. Although the high substitution of MA possessed higher crosslink density, it also led to a decrease in the amount of amino group on chitosan chain, weaking the Schiff base interaction between chitosan and PEGDA, and finally resulting in low mechanical strength. Besides, the increasement of PEGDA (from 2 wt % to 12 wt %) indeed facilitated the gelation process (from 90 s to 36 s), but it was difficult to be further speeded up at high dose of PEGDA because of the limited amino groups on chitosan. The detailed results about different chitosan/PEG hydrogels were summarized in Table S1. Taking the mechanical performance and gelation speed of injectable

hydrogels into consideration, we selected the CSMA2 (2 wt %) and PEGDA (4 wt %) group for *in vitro* cell experiments and *in vivo* implants.

To further evaluate the mechanical performance of the above crosslinked hydrogels, rheological analysis, chemical and physical material characterizations were carried out. The storage modulus (G′) and loss modulus (G″) were recorded under a fixed frequency to demonstrate the viscous and elastic property of different hydrogel groups (Fig. 3a). All samples were in viscous state when they were injected on the plate (G′<G″), and then gradually gelled through Schiff base reaction, which finally in a stable G′ value approximately at 100 Pa (CSMA1-PEGDA), 300 Pa (CSMA2-PEGDA) and 35 Pa (CSMA3-PEGDA) respectively. The higher storage modulus in CSMA2 group further proved that the suitable substitute degree of methacrylic group on chitosan was beneficial to Schiff base crosslinking, which was approximately in accordance with the mechanical testing results (Fig. 2d–f). Besides, the FT-IR spectra at 1650 cm^{-1} and 1720 cm^{-1} ascribed to the stretching vibration of imine group (-CH═N-) and amide group (-CO-NH-) respectively [42], which highlighted the existence of PEGDA in the hydrogels (Fig. 3b and Fig. S5). The high-resolution spectra of XPS also well explained the crosslinking interaction between CSMA and PEGDA (Fig. 3c–e). Each

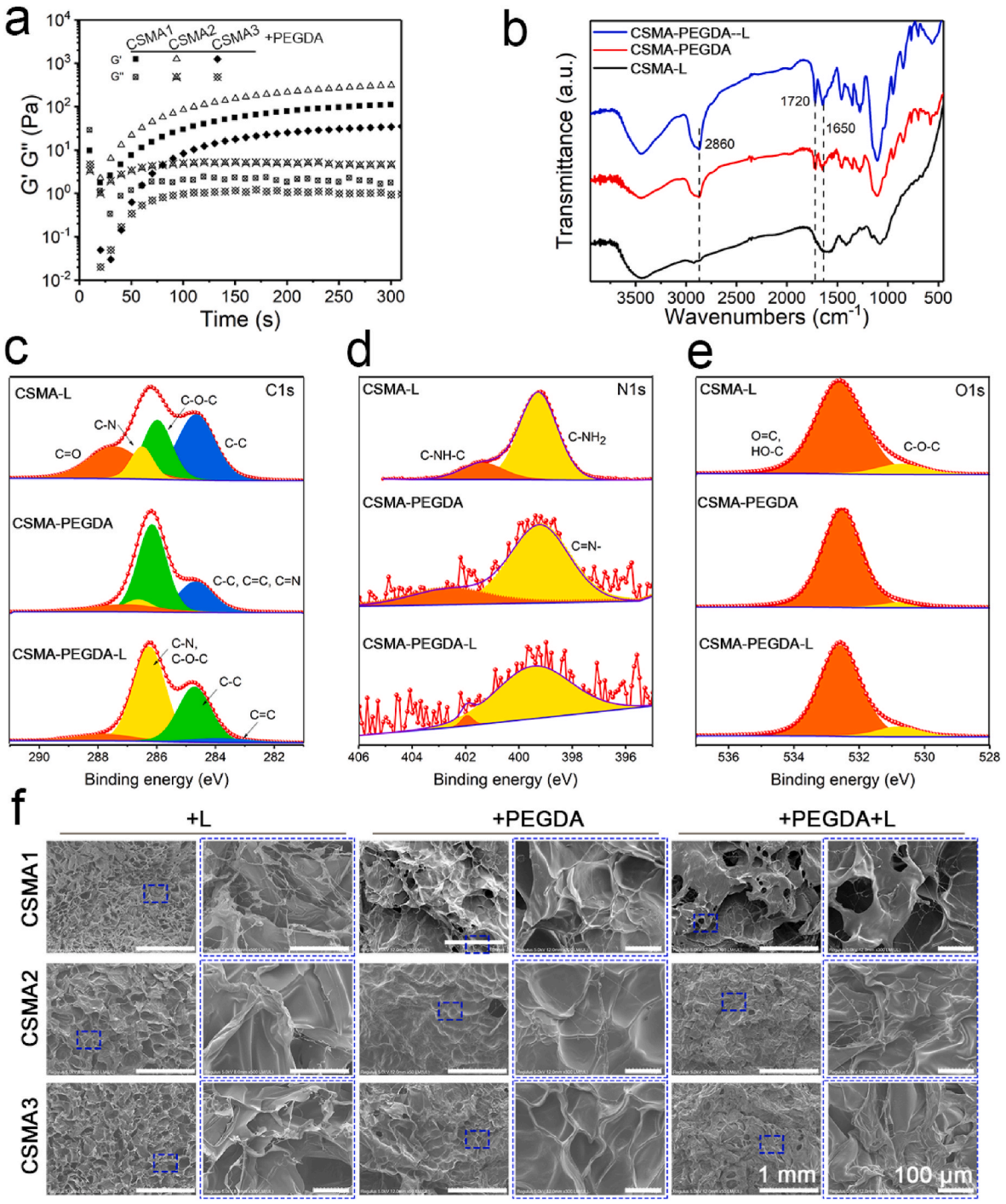

Fig. 3. Characterization on chitosan/PEG hydrogels. Rheology property of different CSMA-PEGDA groups at a fixed strain of 5% (a). FT-IR of three kinds of chitosan/PEG hydrogels (b). XPS high-resolution spectra about C1s (c), N1s (d) and O1s (e) of different chitosan/PEG hydrogels. SEM images of different lyophilized chitosan/PEG hydrogels (f).

sample with 2 wt % solid content was lyophilized to explore the chemical and physical property to explain the enhanced performance of dual network hydrogels. The portion of C–C at 284.7 eV was about 37% in CSMA-L group, obviously higher than CSMA-PEGDA (24%) and CSMA-PEGDA-L (34%). The C═C, π-π* at 283.8 eV, C–O–C at 286.2 eV, and C═O at 287.5 eV shown in CSMA-PEGDA and CSMA-PEGDA-L groups confirmedly indicated the existence of PEGDA and Schiff base reaction (Fig. 3c). This could also be reflected on the variation of N═C at 399.2 eV, N–C at 402.0 eV (Fig. 3d) and O═C at 532.6 eV, C–O–C at 530.6 eV (Fig. 3e). These binding energy results well proved the existence of photo-crosslinking and Schiff base interaction between CSMA and PEGDA. Besides, the morphology variation of different hydrogels

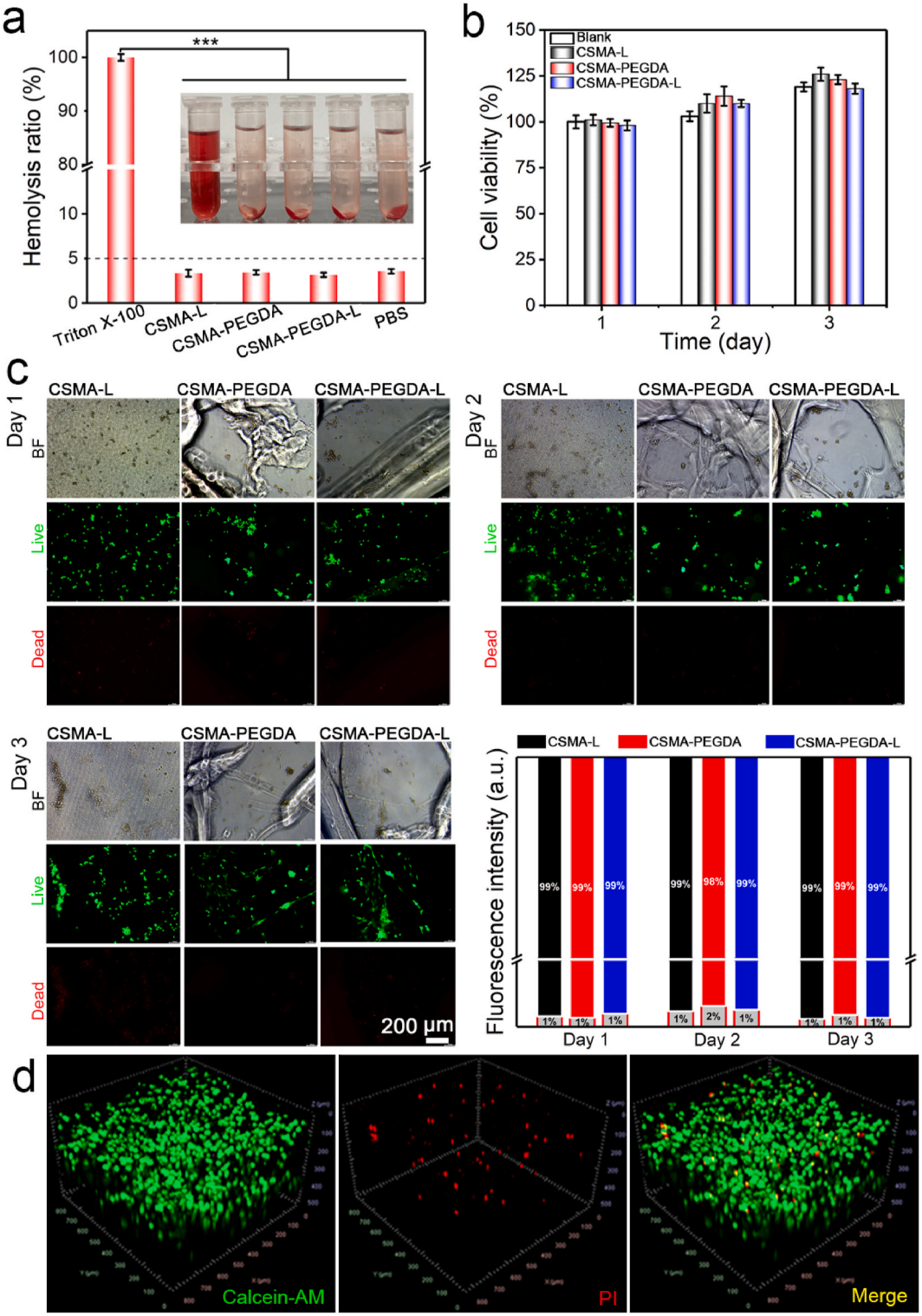

Fig. 4. *In vitro* cell biocompatibility of chitosan/PEG hydrogels. Hemolysis ratio of the chitosan/PEG hydrogels with rat blood cells (a) (n = 5, ***p < 0.001), and cell viability with nucleus pulposus cells in cck-8 kit assay (b) (n = 3). Live/dead staining of nucleus pulposus cells on the surfaces of different chitosan/PEG hydrogels at 1, 2 or 3 days respectively, and the statistics of related fluorescence intensity in each group (c). Live/dead staining of nucleus pulposus cells in CSMA-PEGDA-L hydrogel network with 3D incubation protocol during 24 h.

could also explain the difference about their mechanical strength. All samples possessed porous structures, which became much denser when the substitute degree of MA was increased from CSMA1 to CSMA3, and the Schiff base crosslinked hydrogels also presented the same tendency (Fig. 3f). The high photo-crosslinking density accompanied with Schiff base crosslinking in CSMA2-PEGDA-L group exhibited more denser structure which may explain its outstanding compressive modulus compared to the CSMA1 or CSMA3 groups.

Biocompatibility of implant hydrogels is vital for tissue repair and hemolysis ratio is a typical index to evaluate the blood compatibility before implanted *in vivo* [43]. As shown in Fig. 4a, the photo-crosslinked CSMA-L hydrogel, Schiff base crosslinked CSMA-PEGDA hydrogel, and dual crosslinked CSMA-PEGDA-L hydrogel were all presented low hemolysis ratio (<5%) compared to the positive group 0.1% Triton X-100, indicating an excellent compatibility with blood cell. The NP cells showed greater activity than the blank group through CCK-8 kit assay within three days incubation with different hydrogel leaching solution (Fig. 4b), claiming the low cytotoxicity of the hydrogels. The fluorescence intensity of live/dead staining on cells with 2D co-culture on hydrogel surface also presented good attachment as well as proliferation (Fig. 4c). Although the hydrogel morphology in CSMA-PEGDA or CSMA-PEGDA-L was not intact under bright field, induced by the degradability of hydrogel under cell culture medium, the fluorescence signal was comparable to CSMA-L group. Importantly, the fluorescence density in all groups after three days cultivation showed a low red fluorescence signal (<2%). We also evaluated the degradability of chitosan/PEG hydrogel *in vitro* and found that it remained about 50% weight remaining in lysozyme solution or 90% in PBS during 4 weeks incubation (Fig. S6). Moreover, the cells cultured in the hydrogel network through 3D incubated protocol can greatly simulate the inherent microenvironment of cells, which can better evaluate the biocompatibility of hydrogel [44]. We found that the cells seeded in the CSMA-PEGDA-L hydrogel presented high activity during 3D incubation after 24 h, which may guarantee the activity of NP or AF cells when implanted on rats (Fig. 4d).

Considering the mechanical strength and the cyto-biocompatible property of CSMA and PEGDA hybrid hydrogel, we made it as defect IVD plugging hydrogel (CSMA-PEGDA-L, code as Gel group). The animal experiment schedule and surgery procedure on Sprague Dawley rats with the as-prepared hydrogel were shown in Fig. 5a and b. The degenerated IVD model was created by needle puncture which can stimulate the pathological state of IVD under physiological pressure [45]. Always, radiology and histology on rat's tail were carried out to evaluate the therapeutic efficiency after 4 or 8 weeks. The Micro-CT and its reconstructed 3D model could intuitively show the disc information (Fig. 5c and d). The disc height index was calculated according to the

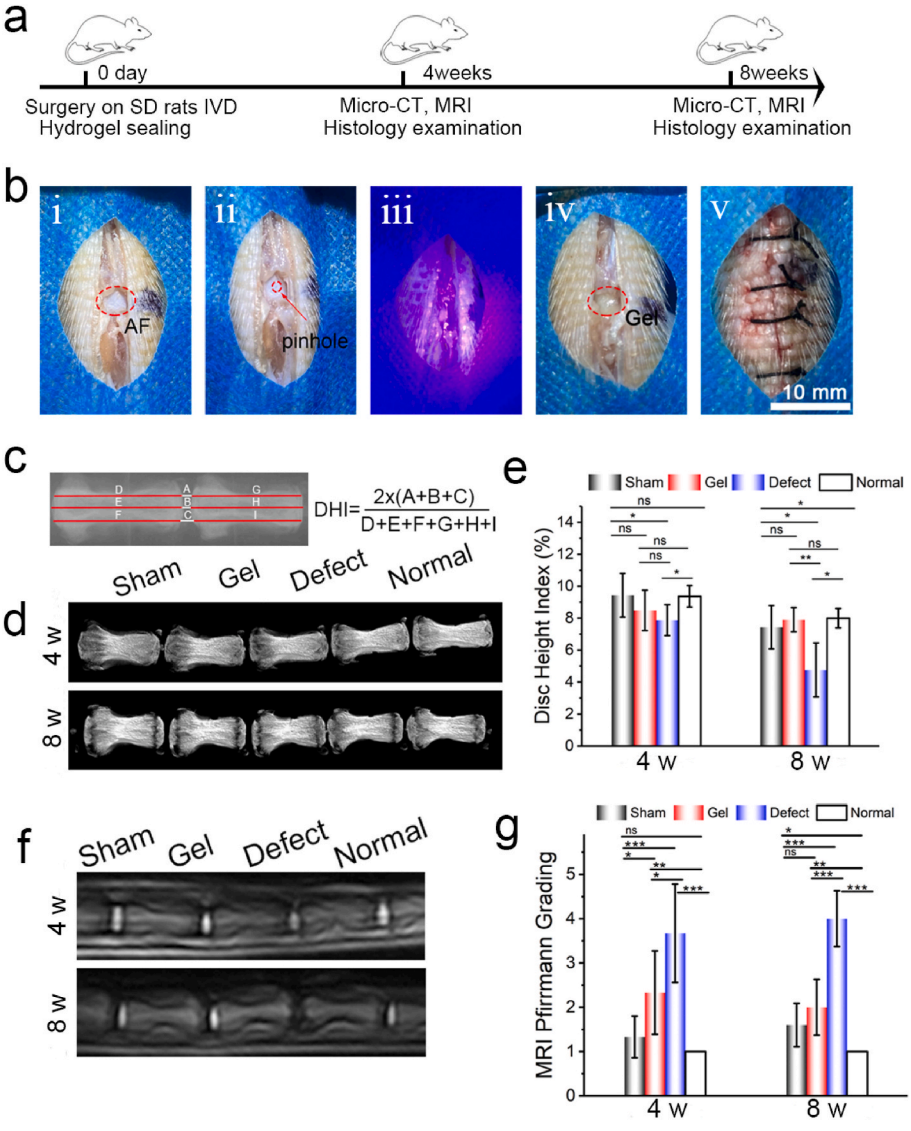

Fig. 5. Animal experiment on IVDD model of the injectable chitosan/PEG hydrogel. Protocol of Gel2 for IVDD model on rat's tail (a). Digital photos of surgery: i, exposure of intervertebral disc; ii, annulus fibers punctured by 26 G needle; iii, blue light 405 nm irradiation on injectable hydrogel; iv, hydrogel sealing on the punctured disc; v, suture after hydrogel formation (b). Micro-CT scanning processing by 2D plane shadow and the disc height index calculation methods (c), 3D reconstruction views of Micro-CT (d) and DHI statistics histogram (e). MRI on sagittal T2 weighted and mapping (f), and Pfirrmann grading scores statistics (g). (n = 5, $p^{***}<0.001$, $p^{**}<0.01$, $p^{*}<0.05$. ns, no significant difference). (For interpretation of the references to colour in this figure legend, the reader is referred to the Web version of this article.)

distance of vertebra and IVD. At the beginning 4 weeks, the IVD in experiment groups were slightly degraded compared with the normal group, but only the defect group showed significant difference with normal or sham group. With time prolonging to 8 weeks, the defect group was further deteriorated which was compared with the hydrogel treatment or control group, while the gel therapeutic IVD was in good disc height index compared with control group (Fig. 5e). These results indicated the hydrogel was able to be a sealing glue at punctured IVD. MRI images on rat's tail in T2-weighted signal can directly reflect the health state of nucleus pulposus by grading the hydration content in IVD. As shown in Fig. 5f, the hyperintense was observed in both normal and sham group, and the gel treatment group was slightly lower than sham group but higher than defect group at 4 weeks. However, the water enrichment state of nucleus pulposus in defect group disappeared while it was still good in the gel or control group at 8 weeks. The Pfirrmann grading analysis on each group showed that the gel treatment indeed prevented the degradation of IVD (Fig. 5g).

To further observe the morphology of NP and AF in different groups, histology analysis on caudal vertebra were conducted (Fig. 6). The lamellae structure of collagen fibers and gelatinous NP was clearly observed both in the sham and normal group at 4 or 8 weeks. The NP was slightly collapsed at 4 weeks as well as 8 weeks in gel group, while it obviously decreased at 4 weeks and significantly deteriorated at 8 weeks in the defect group (Fig. 6a). Safranin O-Fast green was used to directly evaluate the collagen level in IVD. The inner NP, stained in red, was intact both in the sham or normal group, and slightly degenerated in gel group. However, it significantly shrank at 4 weeks and absolutely disappeared at 8 weeks (Fig. 6b). Masson staining, which reflected the fibers of AF [46], also presenting the same tendency as the H&E and Safranin O-Fast green staining (Fig. 6c). Immunohistochemistry on degenerated disc in each group was further used to evaluate the expression of aggrecan and type II collagen after degeneration. As shown in Fig. 7a, aggrecan was highly expressed both in NP and AF, which presented the organized lamellae structure in former and round state in later. The gel group showed an intact morphology of aggrecan compared to the defect group after 8 weeks. Type II collagen existed in NP also distinctly reflected the health state of the gel treated group (Fig. 7b). Histological grade statistics was used to evaluate the degenerated degree of IVD [47], and proved the high grade of the morphology as well as cellularity in the gel treated degenerated disc compared to defect group (Fig. 7c). The H&E staining on main organs of rat also claimed the biosafety of the as-prepared implanted hydrogel (Fig. S7). These results claimed the well ability of the chitosan/PEG hydrogel for preventing the IVD degeneration, and the potential mechanism for IVD repair might be explained as the physical plugging of chitosan/PEG hydrogel (Fig. 7d).

3. Conclusion

A rapidly *in situ* forming injectable chitosan/PEG hydrogel for retarding IVD degeneration was reported. The CSMA-PEGDA could be quickly gelled as injectable hydrogel through Schiff base reaction, which could be further strengthened after blue light irradiation in seconds. The biocompatibility and proliferation to nucleus pulposus cells in the injectable chitosan/PEG hydrogel made it as a potential plugging glue to

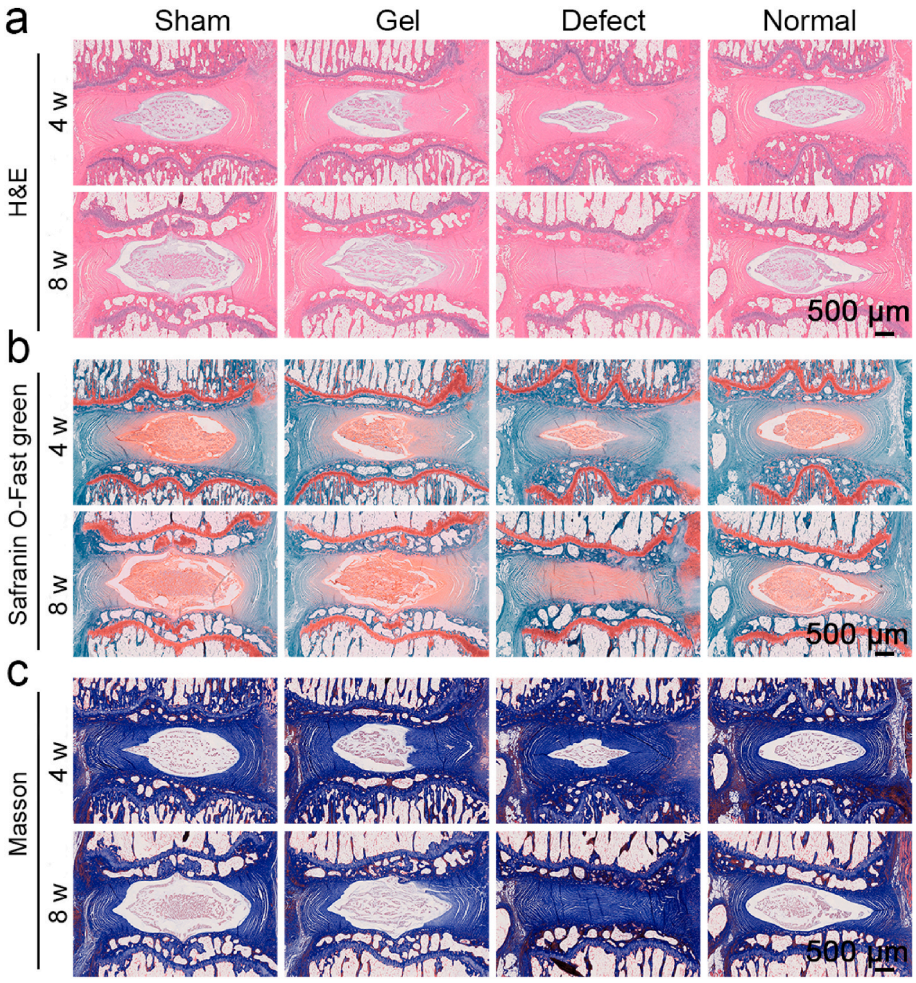

Fig. 6. Histology analysis of intervertebral disc on rat's tail. H&E (a), Safranin O-Fast green (b), Masson (c) staining for morphology evaluation at 4 weeks and 8 weeks respectively. (For interpretation of the references to colour in this figure legend, the reader is referred to the Web version of this article.)

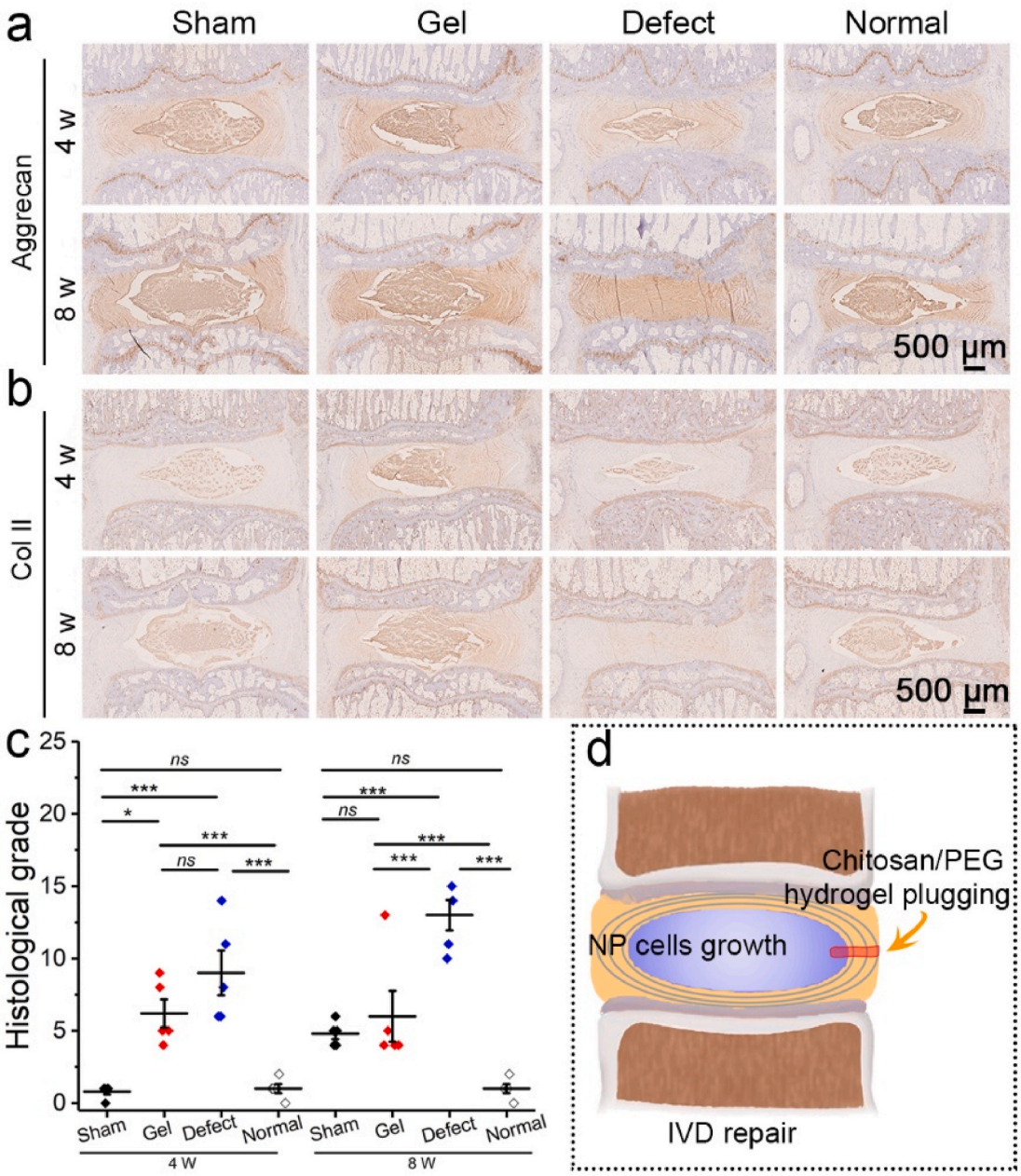

Fig. 7. Immunohistochemistry staining of intervertebral disc on rat's tail. Aggrecan (a) and collagen II (b) to evaluate the state of nucleus pulposus and annulus fibrous. Histological grade statistics by histochemistry and immunohistochemistry evaluation (c) and the overview of the designed chitosan/PEG hydrogel for IVD repair (d). (n = 5, p***<0.001, p**<0.01, p*<0.05, ns, no significant difference).

retard IVD degeneration. *In vivo* experiment on the punctured IVD of rat's tail claimed well therapeutic effect by the chitosan/PEG hydrogel through radiology evaluations such as Micro-CT and MRI at 4 and 8 weeks. Histological analysis including H&E, Safranin O-fast green, Masson staining, and immunohistochemistry staining with aggrecan and type II collagen distinctly showed the positive effect of injectable chitosan/PEG hydrogel on IVD repair. This *in situ* injectable chitosan/PEG hydrogel is expected to as a biomedical sealing glue in tissue repairing.

4. Experiment

Material. Chitosan (viscosity at 100–200 Pa s^{-1}), polyethylene glycol (PEG, molecular weight 2000 g mol^{-1}), methacrylic anhydride, 2, 4, 6-trimethylbenzoyl chloride, dimethyl phenylphosphonite, 2-butanone, and lithium bromide (LiBr), lysozyme (from egg, bioactivity 20000 U/mg) were from Aladdin. 1-(3-Dimethylaminopropyl)-3-ethylcarbodiimide hydrochloride (EDC·HCl), 4-dimethylaminopyridine (DMAP), sodium chloride, sodium bicarbonate, hydrochloric acid, dichloromethane and 4-formylbenzoic acid were from Sinopharm Chemical Reagent Co., Ltd. DMEM with low concentration of glucose (1.0 g/L), penicillin-streptomycin, and PBS were purchased from HyClone. Fetal bovine serum was from Gibco. Triton X-100 and CCK-8 were from Beyotime Biotechnology. Calcein-AM (2 mM) and PI (1.5 mM) were from YEASEN Biotech Co., Ltd. Hematoxylin-Eosin (H&E) staining kit, Safranin O-fast green staining kit, Masson staining kit, anti-collagen II (1:100, rabbit resource), anti-aggrecan (1:100, rabbit resource), goat anti-rabbit IgG conjugated by HRP (1:500) were purchased from Servicebio, China. All reagents were used as received.

4.1. Preparation of light initiator lithium phenyl-2, 4, 6,-trimethylbenoylphosphinate (LAP)

The blue light initiator LAP was synthesized according to the previous report [41]. Briefly, 3.2 g (18 mmol) 2, 4, 6-trimethylbenzoyl chloride was added dropwise into 3.0 g (18 mmol) dimethyl phenylphosphonite in 250 mL round-bottomed flask and stirring 18 h under nitrogen protection at room temperature. 4-folds equivalent for LiBr (6.1 g, 72 mmol) dissolved in 100 mL 2-butanone was added into flask and heated to 50 °C. White solids LAP can be acquired in 10 min and washed three times by 2-butanone. The product was dried in vacuum drying oven overnight and stored in −20 °C for use. ^{1}H NMR (400 MHz, D_2O) of LAP, δ 7.73 (s, 1H), 7.56 (s, 1H), 7.48 (s, 1H), 6.90 (s, 1H), 2.25 (s, 3H), 2.03 (s, 3H).

4.2. Preparation for methacrylate chitosan (CSMA)

1.0 g chitosan (amino groups about 6 mmol) was dissolved in 1 wt% acetic acid with mechanical stirring, and then different mount of methacrylic anhydride was dropwise into chitosan solution to react 12 h under room temperature. The acrylate groups were 5, 10 and 15 mmol in different systems and the ratio of acrylate group to amino group were 0.83, 1.67 and 2.5, respectively. After dialysis by deionized water about 3 days and lyophilization, the water-soluble CSMA with different substituted degrees was obtained as sponge-like products, which were coded as CSMA1, CSMA2 and CSMA3. ^{1}H NMR, (400 MHz, 1%DCl in D_2O): δ 5.61 (s, 1H), 5.30 (s, 1H), 3.68 (d, J = 41.5 Hz, 19H), 2.88 (s, 5H), 2.20–1.60 (m, 13H).

4.3. Preparation for aldehyde group modified polyethylene glycol (PEGDA)

The synthesis of PEGDA was similar to the previous report [48]. Briefly, 3.26 g PEG (hydroxyl groups were about 3.26 mmol) was dissolved in 100 mL anhydrous CH_2Cl_2 with 250 mL round-bottom flask, and then 3.26 mmol 4-carboxybenzaldehyde, 3.26 mmol EDC·HCl, 1.63 mmol DMAP were subsequently added into the flask to react 24 h in 37 °C under N_2 protection. Then 0.1 M HCl, saturated $NaHCO_3$ and NaCl solution were alternatively used to wash the residual reactions, and the organic layer was combined after dried with $MgSO_4$ anhydrous. After rotatory evaporation under vacuum to remove organic solvent, the white wax-like product was acquired and preserved in drier for use. ^{1}H NMR, (400 MHz, $CDCl_3$): δ 10.10 (s, 1H), 8.22 (s, 1H), 7.96 (s, 2H), 4.51 (s, 2H), 3.78 (d, J = 66.6 Hz, 63H).

4.4. Preparation for chitosan based dual crosslink hydrogel modified with polyethylene glycol (CSMA-PEGDA-L)

The single or dual crosslink hydrogels were prepared through two channels pre-mixed syringe. Briefly, 1 mL 2 wt % CSMA and 1 mL PEGDA were loaded in the syringe respectively and then shaped by Schiff base reaction with or without light exposure under 405 nm LED, 25 mW per cm^2. Three kinds of hydrogels were prepared in there: photo-crosslink chitosan hydrogel (CSMA-L), Schiff base crosslink hydrogel (CSMA-PEGDA), and photo-crosslink combined with Schiff base reaction hydrogel (dual crosslink hydrogel, CSMA-PEGDA-L).

4.5. Characterizations for different hydrogels

All hydrogel samples were lyophilized two days under −48 °C before used for FT-IR, XPS, and SEM analysis. In FT-IR (Thermo Fisher Scientific), samples mixed with potassium bromide was compressed into tablets for analysis, detecting the degree of transmittance in range of 400–4000 cm^{-1}. In XPS (Thermo Fisher Scientific K-Alpha), the radiation source is Al Kα (1486.6 eV) with a beam spot at 400 μm and the take-off of the photoelectron was set as 90°. The binding energy was calibrated by C1s 284.8 eV. In SEM (Regulus 800, Japan), all lyophilized hydrogels were coated by a thin film of gold before morphology images capture. Compressive strength on hydrogel samples were carried on mechanical testing machine (Instron 68TM-5, USA) at a speed of 2 mm/min under a 50 N sensor. Rheology property for Schiff base cross-link group hydrogels (CSMA-PEGDA) were performed on rheometer (HAAKE MARS III, Thermo Fisher) with time sweep test model under a fixed strain of 5% at 25 °C. UV–vis spectrophotometer (UV-2600, SHIMADZU) was used to confirm the successful synthesis of PEGDA in water. The Zeta potential value of chitosan and different CSMA samples in diluted solution were obtained by Zetasizer Nano-3000 (Malvern Instruments). The swelling ratios of all the samples were determined by weighting the weight of hydrogel which immersed in water with time prolonging. As for biodegradation, the selected sample was immersed in 1 × PBS which contained 50 μg/mL lysozyme or free, and then shaken with 70 rpm at 37 °C about 4 weeks. The hydrogel samples were weighted after lyophilized to export the degradation curve.

4.6. Hemolysis ratio and degradability of chitosan/PEG hydrogel

Hematocytes were isolated from the whole blood of rats through rinsed with PBS in many times to remove plasma. Three kinds of hydrogels (CSMA-L, CSMA-PEGDA, and CSMA-PEGDA-L) were incubated with blood cells at 37 °C in minutes with 0.1% Triton X-100 or PBS as positive or negative control respectively. Absorption for 100 μL solution in each group at 540 nm with microplate reader were used for evaluated the hemolysis ratio. The biodegradability of CSMA-PEG-L group hydrogel was evaluated in PBS alone or with 50 μg/mL lysozyme in PBS under 37 °C for 4 weeks [49]. The incubated solution was exchanged every two days and samples were weighted after lyophilization.

4.7. Isolation for nucleus pulposus (NP) cells

NP cells were extracted from the caudal vertebras of Sprague-Dawley (SD) rats as following. Tails from SD rats were immersed into 75% ethanol at 10 min after the skin was scrapped. The gel-like NP were acquired after rinsed and isolated the anadesma tissue with 0.1% penicillin-streptomycin containing PBS. The gel-like NP were cut into pieces and centrifugated at 1000 rpm 2 min, and then incubated in 0.5% Trypsin about 30 min which finally blocked by 10% FBS. Resining with 1% penicillin-streptomycin containing PBS many times, and incubated with 0.1% collagenase II in PBS at 37 °C cell incubator about 4 h until no bulk tissue was existed. The NP cells finally can be acquired by incubation with DMEM complete medium.

4.8. Cell incubation of NP cells with hydrogel

4.8.1. Cytotoxicity assay with hydrogel leaching solution

Three kinds of hydrogels were immersed in DMEM at 37 °C about 24 h respectively. After filtrated by 0.22 μm filter and diluted into 50 mg/mL, 5 × 10^3 NP cell were co-cultured with the leaching solution in 96 well plates for 1, 2, or 3 days respectively. 10 μL CCK-8 kit was mixed in 100 μL medium for another 1 h incubation before 450 nm detected on microplate reader.

4.8.2. 2D cells incubation on hydrogel surface

400 μL precursor of three kinds of hydrogels were put into 24 well plates with another 2 min light exposure for gelation. 2 mL DMEM were added on hydrogel and incubation with 10 min before cells loading. 1 × 10^5 NPs cell were seeded on hydrogel surface for incubation at 1, 2, or 3 days respectively. Then 1 mL Calcein-AM and PI with a staining concentration at 2 μM and 4.5 μM in 1 × assay buffer respectively was added into each hole for another 30 min incubation before observing under Fluorescent Inverted Microscope.

4.8.3. 3D cells incubation in hydrogel network

200 μL sterilized CSMA precursor (0.2 wt% LAP) was spread on the bottom of 3.5 cm diameter confocal culture disc. Then 5×10^5 NP cells were resuspended with 200 μL DMEM with PEGDA (0.2 wt% LAP) contained 40 μL FBS and uniformly mixed with CSMA. Blue light (405 nm) was used for the double network formation, and 1 mL DMEM was pre-soaked into culture disc about 10 min. Another 1 mL culture medium was replaced for incubation about 24 h. After that, 1 mL Calcein-AM and PI with a working concentration at 2 μM and 4.5 μM in 1 × assay buffer was added into culture disc, and further detected by confocal laser scanning microscope (CLSM, Zeiss) in Z stack model with a thickness at 5 μm in each slice.

4.9. Animal surgery with injectable hydrogel

Twelves Sprague-Dawley rats (male, average weight 300–350 g, 8 weeks old) were randomly categorized into two groups, and further experiments were ethically approved by animal experimentation committee of Southern University of Science and Technology (SUSTech-JY202111008). After anaesthetized by isoflurane, the caudal vertebrae on 3 to 7 were exposure by surgery knife on each rat. And then four intervertebral discs were used as experimental object, which coded as sham group (Co3/4), gel group (Co4/5), defect group (Co5/6), and normal group (Co6/7) respectively. Briefly, the anadesma between two caudal vertebrae was cut off without further destruction on annulus fiber in sham group. The intervertebral disc both in gel group and defect group were acupunctured by 26 G needle with rotating 360° after passing through the annulus and holding for 30 s. The hydrogel precursor was coated on the pinhole in gel group with 405 nm blue light irradiation 2 min while no further treatment in defect group. The incision in normal group was directly closed by 6–0 sutures after exposure by surgery knife. All animal tails were daily wiped with iodophor and administration of 500 μL penicillin solution (100 mg/mL) on each rat through intraperitoneal injection to prevent infection in first week.

4.10. Radiology and MRI analysis

After recovery at 4 or 8 weeks, all rats were anaesthetized by Zoletil®50 (50 mg/kg) through intramuscular injection for radiology and MRI evaluations. Micro computed tomography (Micro-CT, SkyScan126, Bruker) with Al 1 mm as filter and magnetic resonance imaging (MRI, 1.5 T vPetMR, GSMED) with slice thickness in 3 mm were used to evaluate the condition of degenerated IVD. The reconstruction from the batch scan can intuitively reflect the IVD health condition, which can further calculate the disc high index (DHI) according to the previous report [50]. T2-weight and mapping in sagittal sections were performed and further evaluated by Pfirrmann grading method [51].

4.11. Histological evaluation

All the rats were sacrificed after 4 or 8 weeks. The experimental tails with the detached skin were separated from the rat, and fixed by 4% paraformaldehyde solution for 48 h. After decalcified in 10% EDTA phosphate solution about one month (decalcified solution was replaced every 3 days) and dehydrated by gradient alcohol, the sample was embedded with paraffin and then sliced for hematoxylin and eosin (H&E), Safranin O-Fast green (S–O) and Masson solution staining. Sagittal sections on each experimental IVD were obtained with 5 μm thickness on slide for further staining analysis. Immunohistochemistry staining for type II collagen and aggrecan were also performed to evaluate the treatment effect of the as-prepared hydrogel. Briefly, the tissue slice was blocked with 3% BSA about 30 min under room temperature. After removed the sealing fluid, the samples were incubated with anti-collagen II or anti-aggrecan at 4 °C overnight. With another 1 h incubation with goat anti-rabbit IgG conjugated by HRP after rinsed by PBS, the samples were fixed on slide for further observation. H&E staining for heart, liver, spleen, lung and kidney on experimental rats were also acquired to evaluate the biocompatibility of hydrogel *in vivo*. All histological staining experiment protocols were performed according to previous reports [47,52].

5. Statistical analysis

All data were analyzed through one-way analysis of variance (ANOVA) with Tukey's comparisons tests to evaluate the significant difference of each group. Significance threshold was set as $^*p < 0.05$, $^{**}p < 0.0.1$, $^{***}p < 0.001$ for all results.

Credit authors statement

Lin Huang: Conceptualization, Methodology, Data curation, Writing – original draft.**Wantao Wang**: Methodology, Data curation, Writing – original draft.**Yiwen Xian**: Formal analysis, Methodology. **Lei Liu**: Methodology, Investigation.**Jinghao Fan**: Methodology, Investigation. **Hongmei Liu**: Funding acquisition, Project administration, Supervision, Resources, Writing – review & editing.**Zhaomin Zheng**: Project administration, Supervision, Resources, Writing – review & editing. **Decheng Wu**: Funding acquisition, Project administration, Supervision, Resources, Writing – review & editing.

Declaration of competing interest

The authors declare no competing financial interest.

Data availability

Data will be made available on request.

Acknowledgement

This work is supported by the Ministry of Science and Technology of China (2020YFA0908900), National Natural Science Foundation of China (21935011 and 21725403), Shenzhen Science and Technology Innovation Commission (KQTD20200820113012029 and JSGG20200225151916021), Shenzhen Basic Research Project (JCYJ20220530114409020), and Guangdong Provincial Key Laboratory of Advanced Biomaterials (2022B1212010003).

Appendix A. Supplementary data

Supplementary data related to this article can be found at https://doi.org/10.1016/j.mtbio.2023.100752.

References

[1] J. Hartvigsen, M.J. Hancock, A. Kongsted, Q. Louw, M.L. Ferreira, S. Genevay, D. Hoy, J. Karppinen, G. Pransky, J. Sieper, R.J. Smeets, M. Underwood, R. Buchbinder, J. Hartvigsen, D. Cherkin, N.E. Foster, C.G. Maher, M. Underwood, M. van Tulder, J.R. Anema, R. Chou, S.P. Cohen, L. Menezes Costa, P. Croft, M. Ferreira, P.H. Ferreira, J.M. Fritz, S. Genevay, D.P. Gross, M.J. Hancock, D. Hoy, J. Karppinen, B.W. Koes, A. Kongsted, Q. Louw, B. Öberg, W.C. Peul, G. Pransky, M. Schoene, J. Sieper, R.J. Smeets, J.A. Turner, A. Woolf, What low back pain is and why we need to pay attention, Lancet 391 (10137) (2018) 2356–2367.

[2] G.E. Hicks, N. Morone, D.K. Weiner, Degenerative lumbar disc and facet disease in older adults: prevalence and clinical correlates, Spine 34 (12) (2009) 1301–1306. Phila Pa 1976.

[3] K.D. Hudson, M. Alimi, P. Grunert, R. Härtl, L.J. Bonassar, Recent advances in biological therapies for disc degeneration: tissue engineering of the annulus fibrosus, nucleus pulposus and whole intervertebral discs, Curr. Opin. Biotechnol. 24 (5) (2013) 872–879.

[4] D. Wu, G. Li, X. Zhou, W. Zhang, H. Liang, R. Luo, K. Wang, X. Feng, Y. Song, C. Yang, Repair strategies and bioactive functional materials for intervertebral disc, Adv. Funct. Mater. (2022), 2209471.

[5] K.-S. Suk, H.-M. Lee, S.-H. Moon, N.-H. Kim, Recurrent lumbar disc herniation: results of operative management, J. Spine 26 (6) (2001) 672–676.

[6] P. Heindel, A. Tuchman, P.C. Hsieh, M.H. Pham, A. D'Oro, N.N. Patel, A.M. Jakoi, R. Hah, J.C. Liu, Z. Buser, Reoperation rates after single-level lumbar discectomy, J. Spine 42 (8) (2017) 496–501.

[7] C.-J. Chiang, C.-K. Cheng, J.-S. Sun, C.-J. Liao, Y.-H. Wang, Y.-H. Tsuang, The effect of a new anular repair after discectomy in intervertebral disc degeneration: an experimental study using a porcine spine Model, Spine 36 (10) (2011) 761–769.

[8] I.L. Mohd Isa, S.A. Mokhtar, S.A. Abbah, M.B. Fauzi, A. Devitt, A. Pandit, Intervertebral disc degeneration: biomaterials and tissue engineering strategies toward precision medicine, Adv Healthc Mater 11 (13) (2022), e2102530.

[9] R.D. Bowles, H.H. Gebhard, R. Hartl, L.J. Bonassar, Tissue-engineered intervertebral discs produce new matrix, maintain disc height, and restore biomechanical function to the rodent spine, Proc. Natl. Acad. Sci. U. S. A. 108 (32) (2011) 13106–13111.

[10] T.J. DiStefano, J.O. Shmukler, G. Danias, J.C. Iatridis, The functional role of interface tissue engineering in annulus fibrosus repair: bridging mechanisms of hydrogel integration with regenerative outcomes, ACS Biomater. Sci. Eng. 6 (12) (2020) 6556–6586.

[11] S.E. Malli, P. Kumbhkarn, A. Dewle, A. Srivastava, Evaluation of tissue engineering approaches for intervertebral disc regeneration in relevant animal models, ACS Appl. Bio Mater. 4 (11) (2021) 7721–7737.

[12] T.J. DiStefano, J.O. Shmukler, G. Danias, T. Di Pauli von Treuheim, W.W. Hom, D. A. Goldberg, D.M. Laudier, P.R. Nasser, A.C. Hecht, S.B. Nicoll, J.C. Iatridis, Development of a two-part biomaterial adhesive strategy for annulus fibrosus repair and ex vivo evaluation of implant herniation risk, Biomaterials 258 (2020), 120309.

[13] S.R. Sloan Jr., C. Wipplinger, S. Kirnaz, R. Navarro-Ramirez, F. Schmidt, D. McCloskey, T. Pannellini, A. Schiavinato, R. Härtl, L.J. Bonassar, Combined nucleus pulposus augmentation and annulus fibrosus repair prevents acute intervertebral disc degeneration after discectomy, Sci. Transl. Med. 12 (534) (2020), eaay2380.

[14] J. Chen, H. Zhu, Y. Zhu, C. Zhao, S. Wang, Y. Zheng, Z. Xie, Y. Jin, H. Song, L. Yang, J. Zhang, J. Dai, Z. Hu, H. Wang, Injectable self-healing hydrogel with siRNA delivery property for sustained STING silencing and enhanced therapy of intervertebral disc degeneration, Bioact. Mater. 9 (2021) 29–43.

[15] F. Tao, Y. Cheng, X. Shi, H. Zheng, Y. Du, W. Xiang, H. Deng, Applications of chitin and chitosan nanofibers in bone regenerative engineering, Carbohydr. Polym. 230 (2020), 115658.

[16] J.A. Burdick, G.D. Prestwich, Hyaluronic acid hydrogels for biomedical applications, Adv. Mater. 23 (12) (2011) H41–H56.

[17] Y. Li, X. Wang, Y.N. Fu, Y. Wei, L. Zhao, L. Tao, Self-adapting hydrogel to improve the therapeutic effect in wound-healing, ACS Appl. Mater. Interfaces 10 (31) (2018) 26046–26055.

[18] Y.N. Fu, Y. Li, B. Deng, Y. Yu, F. Liu, L. Wang, G. Chen, L. Tao, Y. Wei, X. Wang, Spatiotemporally dynamic therapy with shape-adaptive drug-gel for the improvement of tissue regeneration with ordered structure, Bioact. Mater. 8 (2022) 165–176.

[19] Y. Liu, S.H. Lin, W.T. Chuang, N.T. Dai, S.H. Hsu, Biomimetic strain-stiffening in chitosan self-healing hydrogels, ACS Appl. Mater. Interfaces 14 (14) (2022) 16032–16046.

[20] J. Li, A.D. Celiz, J. Yang, Q. Yang, I. Wamala, W. Whyte, B.R. Seo, N.V. Vasilyev, J. J. Vlassak, Z. Suo, D.J. Mooney, Tough adhesives for diverse wet surfaces, Science 357 (6349) (2017) 378.

[21] B.R. Freedman, A. Kuttler, N. Beckmann, S. Nam, D. Kent, M. Schuleit, F. Ramazani, N. Accart, A. Rock, J. Li, Enhanced tendon healing by a tough hydrogel with an adhesive side and high drug-loading capacity, Nat. Biomed. Eng. (2022) 1–13.

[22] X. Du, Y. Liu, H. Yan, M. Rafique, S. Li, X. Shan, L. Wu, M. Qiao, D. Kong, L. Wang, Anti-infective and pro-coagulant chitosan-based hydrogel tissue adhesive for sutureless wound closure, Biomacromolecules 21 (3) (2020) 1243–1253.

[23] B.D. Zheng, J. Ye, Y.C. Yang, Y.Y. Huang, M.T. Xiao, Self-healing polysaccharide-based injectable hydrogels with antibacterial activity for wound healing, Carbohydr. Polym. 275 (2022), 118770.

[24] L. Upadhyaya, J. Singh, V. Agarwal, R.P. Tewari, The implications of recent advances in carboxymethyl chitosan based targeted drug delivery and tissue engineering applications, J. Contr. Release 186 (2014) 54–87.

[25] A.H. Pandit, S. Nisar, K. Imtiyaz, M. Nadeem, N. Mazumdar, M.M.A. Rizvi, S. Ahmad, Injectable, self-healing, and biocompatible N,O-carboxymethyl chitosan/multialdehyde guar gum hydrogels for sustained anticancer drug delivery, Biomacromolecules 22 (9) (2021) 3731–3745.

[26] S. Wang, J. Chi, Z. Jiang, H. Hu, C. Yang, W. Liu, B. Han, A self-healing and injectable hydrogel based on water-soluble chitosan and hyaluronic acid for vitreous substitute, Carbohydr. Polym. 256 (2021), 117519.

[27] B. Gong, X. Zhang, A.A. Zahrani, W. Gao, G. Ma, L. Zhang, J. Xue, Neural tissue engineering: from bioactive scaffolds and in situ monitoring to regeneration, Explorations 2 (3) (2022), 20210035.

[28] L. Huang, C.-J. Liu, Progress for the development of antibacterial surface based on surface modification technology, Supramol. Mater. 1 (2022), 100008.

[29] P. King, J. Ward, Radiation chemistry of aqueous poly (ethylene oxide) solutions. I, J. Polym. Sci. 1 Polym. Chem. 8 (1) (1970) 253–262.

[30] J. Zhu, Bioactive modification of poly(ethylene glycol) hydrogels for tissue engineering, Biomaterials 31 (17) (2010) 4639–4656.

[31] H. Ye, Y. Xian, S. Li, C. Zhang, D. Wu, In situ forming injectable gamma-poly (glutamic acid)/PEG adhesive hydrogels for hemorrhage control, Biomater. Sci. 10 (15) (2022) 4218–4227.

[32] F. Song, Y. Kong, C. Shao, Y. Cheng, J. Lu, Y. Tao, J. Du, H. Wang, Chitosan-based multifunctional flexible hemostatic bio-hydrogel, Acta Biomater. 136 (2021) 170–183.

[33] R. Dong, X. Zhao, B. Guo, P.X. Ma, Self-Healing conductive injectable hydrogels with antibacterial activity as cell delivery carrier for cardiac cell therapy, ACS Appl. Mater. Interfaces 8 (27) (2016) 17138–17150.

[34] H.Y. Jung, P. Le Thi, K.H. HwangBo, J.W. Bae, K.D. Park, Tunable and high tissue adhesive properties of injectable chitosan based hydrogels through polymer architecture modulation, Carbohydr. Polym. 261 (2021), 117810.

[35] Y. Liu, C.W. Wong, S.W. Chang, S.H. Hsu, An injectable, self-healing phenol-functionalized chitosan hydrogel with fast gelling property and visible light-crosslinking capability for 3D printing, Acta Biomater. 122 (2021) 211–219.

[36] H. Wang, X. Wang, D. Wu, Recent advances of natural polysaccharide-based double-network hydrogels for tissue repair, Chem. Asian J. 17 (17) (2022), e202200659.

[37] W. Han, B. Zhou, K. Yang, X. Xiong, S. Luan, Y. Wang, Z. Xu, P. Lei, Z. Luo, J. Gao, Y. Zhan, G. Chen, L. Liang, R. Wang, S. Li, H. Xu, Biofilm-inspired adhesive and antibacterial hydrogel with tough tissue integration performance for sealing hemostasis and wound healing, Bioact. Mater. 5 (4) (2020) 768–778.

[38] C.K.S. Pillai, W. Paul, C.P. Sharma, Chitin and chitosan polymers: chemistry, solubility and fiber formation, Prog. Polym. Sci. 34 (7) (2009) 641–678.

[39] B. Li, L. Wang, F. Xu, X. Gang, U. Demirci, D. Wei, Y. Li, Y. Feng, D. Jia, Y. Zhou, Hydrosoluble, UV-crosslinkable and injectable chitosan for patterned cell-laden microgel and rapid transdermal curing hydrogel in vivo, Acta Biomater. 22 (2015) 59–69.

[40] Y. Shen, H. Tang, X. Huang, R. Hang, X. Zhang, Y. Wang, X. Yao, DLP printing photocurable chitosan to build bio-constructs for tissue engineering, Carbohydr. Polym. 235 (2020), 115970.

[41] B.D. Fairbanks, M.P. Schwartz, C.N. Bowman, K.S. Anseth, Photoinitiated polymerization of PEG-diacrylate with lithium phenyl-2,4,6-trimethylbenzoylphosphinate: polymerization rate and cytocompatibility, Biomaterials 30 (35) (2009) 6702–6707.

[42] X. Yang, G. Liu, L. Peng, J. Guo, L. Tao, J. Yuan, C. Chang, Y. Wei, L. Zhang, Highly efficient self-healable and dual responsive cellulose-based hydrogels for controlled release and 3D cell culture, Adv. Funct. Mater. 27 (40) (2017), 1703174.

[43] S. Henkelman, G. Rakhorst, J. Blanton, W. van Oeveren, Standardization of incubation conditions for hemolysis testing of biomaterials, Mater. Sci. Eng. C 29 (5) (2009) 1650–1654.

[44] E. Carletti, A. Motta, C. Migliaresi, Scaffolds for tissue engineering and 3D cell culture, in: J.W. Haycock (Ed.), 3D Cell Culture: Methods and Protocols, Humana Press, Totowa, NJ, 2011, pp. 17–39, https://doi.org/10.1007/978-1-60761-984-0_2.

[45] Y. Takeoka, T. Yurube, K. Morimoto, S. Kunii, Y. Kanda, R. Tsujimoto, Y. Kawakami, N. Fukase, T. Takemori, K. Omae, Y. Kakiuchi, S. Miyazaki, K. Kakutani, T. Takada, K. Nishida, M. Fukushima, R. Kuroda, Reduced nucleotomy-induced intervertebral disc disruption through spontaneous spheroid formation by the Low Adhesive Scaffold Collagen (LASCol), Biomaterials 235 (2020), 119781.

[46] Z. Liao, H. Liu, L. Ma, J. Lei, B. Tong, G. Li, W. Ke, K. Wang, X. Feng, W. Hua, Engineering extracellular vesicles restore the impaired cellular uptake and attenuate intervertebral disc degeneration, ACS Nano 15 (9) (2021) 14709–14724.

[47] Z. Liao, S. Li, S. Lu, H. Liu, G. Li, L. Ma, R. Luo, W. Ke, B. Wang, Q. Xiang, Y. Song, X. Feng, Y. Zhang, X. Wu, W. Hua, C. Yang, Metformin facilitates mesenchymal stem cell-derived extracellular nanovesicles release and optimizes therapeutic efficacy in intervertebral disc degeneration, Biomaterials 274 (2021), 120850.

[48] Y. Bu, L. Zhang, J. Liu, L. Zhang, T. Li, H. Shen, X. Wang, F. Yang, P. Tang, D. Wu, Synthesis and properties of hemostatic and bacteria-responsive in situ hydrogels for emergency treatment in critical situations, ACS Appl. Mater. Interfaces 8 (20) (2016) 12674–12683.

[49] T. Wu, L. Huang, J. Sun, J. Sun, Q. Yan, B. Duan, L. Zhang, B. Shi, Multifunctional chitin-based barrier membrane with antibacterial and osteogenic activities for the treatment of periodontal disease, Carbohydr. Polym. 269 (2021), 118276.

[50] J. Bian, F. Cai, H. Chen, Z. Tang, K. Xi, J. Tang, L. Wu, Y. Xu, L. Deng, Y. Gu, W. Cui, L. Chen, Modulation of local overactive inflammation via injectable hydrogel microspheres, Nano Lett. 21 (6) (2021) 2690–2698.

[51] C.W. Pfirrmann, A. Metzdorf, M. Zanetti, J. Hodler, N. Boos, Magnetic resonance classification of lumbar intervertebral disc degeneration, J. Spine 26 (17) (2001) 1873–1878.

[52] L. Huang, X. Yang, L. Deng, D. Ying, A. Lu, L. Zhang, A. Yu, B. Duan, Biocompatible chitin hydrogel incorporated with PEDOT nanoparticles for peripheral nerve repair, ACS Appl. Mater. Interfaces 13 (14) (2021) 16106–16117.